Finite Elements in Analysis and Design 46 (2010) 732–742

Contents lists available at ScienceDirect

Finite Elements in Analysis and Design

journal homepage: www.elsevier.com/locate/finel

Multilayered plate elements for the analysis of multifield problems ☆

E. Carrera, P. Nali *

Aerospace Department, Politecnico di Torino, Corso Duca degli Abruzzi, 24, 10129 Torino, Turin, Italy

ARTICLE INFO

Article history:
Received 1 December 2008
Received in revised form
14 December 2009
Accepted 24 April 2010
Available online 14 May 2010

Keywords:
Finite elements
Multilayered plates
Multifield problems
Refined models
Smart structures

ABSTRACT

This work deals with advanced finite element (FE) formulations for the analysis of multilayered structures in the case of multifield problems. The following four fields are considered: mechanical, thermal, electrical and magnetic. Constitutive equations, in terms of coupled mechanical–thermal–electrical–magnetic field variables, are obtained on the basis of a thermodynamic approach. The four-field principle of virtual displacements is employed to derive FE matrices. Three-fields, two-fields as well as pure mechanical problems have been discussed as relevant particular cases. A condensed notation, known as Carrera unified formulation, has been employed to establish a comprehensive two-dimensional modeling with variable kinematic features. Layer-wise/equivalent single layers plate elements have been developed according to linear up to fourth-order expansion in the layer/plate thickness directions. FE matrices have been obtained in terms of a few fundamental nuclei whose dimension is 6×6 for the full four fields case. Numerical results show the effectiveness of the proposed implementation by encompassing various static and dynamic multifield plate problems.

1. Introduction

Conventional and unconventional spacecraft constructions have constantly been characterized by an extensive use of multilayered structures (MLSs). First, layers of metallic/ceramic materials have been adopted as thermal protection systems. Recently, advanced composite materials have been used to build large parts of spacecrafts. Metallic and composite structures can be considered as *conventional* multilayered application; these are, in fact, largely applied in space technology. Moreover, other *unconventional* MLSs are under consideration for their possible use for the next generation of spacecrafts: smart structures (in which piezoelectric layers or patches are embedded in the structure) and inflatable structures (made by many layers of very different materials). Accurate structural modeling of multilayered made structures when subjected to various fields (mechanical, thermal, electrical) is a crucial point for the structural analyst. The possibility of building a real time control for smart structures for the practical space structures is still to be demonstrated. Available commercial software, which has not been designed for the analysis of the structures above mentioned, can experience some difficulties in their simulation.

There are many open problems concerning the mechanical modeling of these structures. Theories and computational models implemented in available codes have been, in fact, mostly devoted to simulation of traditional one-layered structures. Amendments to these findings are mandatory to capture the effective mechanical, thermal and electrical fields in each layer.

A number of requirements must be taken into account for an accurate analysis of multifield problems (MFPs) and MLSs. The following points are relevant to the aim of this paper: (1) the constitutive equations must be derived in a consistent form; (2) the coupling among the various fields should be accurately described; (3) interlayer continuity of the relevant variables must be guaranteed; (4) the employed kinematic model must be rich enough to describe the localized through-the-thickness-distribution of the involved variables in the various layers. Reference to a thermodynamic basis is mandatory for point 1 [1]. For the fulfillment of point 2, the constitutive relations are coupled. For the general case, thermo-electro-magnetic–mechanical coupling can be included in the formulation [2]. As far as point 3 is concerned, it should be pointed out that a classical choice of primary variables for the various fields could violate some interlaminar continuities. This is the case of transverse shear and normal stresses, which must be continuous at each layer interface because of equilibrium reasons. Such continuity is not enforced in classical modeling which only makes use of displacement variables [3]. The same could be said for transverse electrical displacements or transverse magnetic inductance [4,5]; further mixed variational statements have been recently discussed in [2].

☆ The content of this paper has been partially presented at the 16th AIAA/ASME/AHS Adaptive Structures Conference, 7–10 April 2008, Schaumburg, IL.

* Corresponding author. Tel.: +39 011 564 6869; fax: +39 011 564 6899.
E-mail address: pietro.nali@polito.it (P. Nali).

0168-874X/$ - see front matter © 2010 Elsevier B.V. All rights reserved.
doi:10.1016/j.finel.2010.04.001

Concerning point 4, it is well known that the use of variable kinematic models is mandatory in MLSs subjected to MFP loadings. These loadings, in fact, have an *isotropic/anisotropic* and *localized* nature. For instance, the thermal field, being scalar, is isotropic by definition while the electrical and magnetic fields, being vectorial, can be isotropic or anisotropic. Loadings from these fields are completely different from those from mechanical cases. Consequently, kinematic models that were originally proposed for plate and shell structures subjected to mechanical loading could undergo difficulties analyzing MFPs. Modelings that permit the use of both equivalent single layer models (ESLM) and layer wise models (LWM) are in these cases.

Recent research works carried out at Politecnico di Torino by Carrera unified formulation (CUF) for plate and shell analyses have established a hierarchic finite element formulation for MLSs subjected to multifield loading (e.g. mechanical–thermal–electrical–magnetic) [2,4,5]. This approach consists in a valuable tool for the analysis of both conventional and unconventional structures. Shell applications are proposed in [6].

Starting from the work [2], which is mainly theoretical and proposes a wide set of PVD (principle of virtual displacements) and RMVT (Reissner mixed variational theorem) multifield variational statements, this paper is focused on multilayered plate elements based on the extended four-field form of the PVD. Applying the PVD, CUF leads to a 6×6 fundamental nucleus which reduces as particular cases to thermo-mechanical, electro-mechanical, magneto-mechanical and pure mechanical problems. A set of multifield finite elements is obtained and assessed through convergence studies and benchmarking with exact 3D solutions. Particular attention is dedicated to thermo-mechanical fully coupled analysis.

Concerning the piezoelectric problem, some analytical and FEM results are provided in works [4,5], using the RMVT. Electro-mechanical modeling illustrated in this paper refers to the PVD and then leads to FEs with a smaller number of DOFs respect to RMVT. The piezoelectric problem is considered as a particular subcase of the four-field fully coupled analysis.

The paper is organized as it follows: the used four-fields variational statements are discussed in Section 2; FE equations in terms of fundamental nuclei are obtained in Section 3. FE development has been coded in a FORTAN90 environment. Resulting code has been named MUL2 (*MUL*ti layered structures and *MUL*tifield problems) and analyses made have been reported in Section 4.

2. Extension of PVD to four field problems

2.1. Constitutive equations

The constitutive equations are written according to thermodynamic basis described in [1,7], and extended in [8,2] for linear problems. Standard tensor notation is used and Einstein's summation convention is implied over repeated indices. A Cartesian reference system is considered. A set of intensive variables θ, ε, E and H, which are, respectively, the increment in temperature, strain, electric field and magnetic field, are first assumed as independent variables. The relevant thermodynamic function is the Gibbs free energy per unit of volume G [1], which is here extended to include the magnetic field:

$$G = U + \sigma_{ij}\varepsilon_{ij} - \theta\eta - E_i D_i - H_i B_i, \tag{1}$$

where U is the internal energy per unit of volume (function of η,ε_{ij},D_i and B_i); η is the variation of entropy per unit of volume; σ_{ij} is the stress tensor; D_i is the electrical displacements vector; B_i is the magnetic inductance vector. According to the development in [2], the following form of the constitutive equations for the four-field problem is obtained:

$$\begin{aligned}
\eta &= \frac{\rho}{\theta_{ref}} C^{\varepsilon,E,H}\theta + \lambda_{ij}^{E,H}\varepsilon_{ij} + p_i^{\varepsilon,H}E_i + r_i^{\varepsilon,E}H_i,\\
\sigma_{ij} &= -\lambda_{ij}^{E,H}\theta + C_{ijlm}^{\theta,E,H}\varepsilon_{lm} - e_{ijl}^{\theta,H}E_l - q_{ijl}^{\theta,E}H_l,\\
D_l &= p_l^{\varepsilon,H}\theta + e_{lij}^{\theta,H}\varepsilon_{ij} + \varepsilon_{lm}^{\theta,\varepsilon,H}E_m + d_{lm}^{\theta,\varepsilon}H_m,\\
B_l &= r_l^{\varepsilon,E}\theta + q_{lij}^{\theta,E}\varepsilon_{ij} + d_{lm}^{\theta,\varepsilon}E_m + \mu_{lm}^{\theta,\varepsilon,E}H_m,
\end{aligned} \tag{2}$$

where ρ is the material density; C is the specific heat per unit mass; θ_{ref} is the temperature of reference; C_{ijlm} is the elastic coefficients—Hooke's law; ε_{ij} is the permittivity coefficients; μ_{ij} is the magnetic permeability coefficients; λ_{ij} is the stress-temperature coefficients; p_i is the pyroelectric coefficients; e_{lij} is the piezoelectric coefficients; r_i is the pyromagnetic coefficients; q_{lij} is the piezomagnetic coefficients; d_i is the magneto-electric coupling coefficients. Superscripts in Eq. (2) refer to the quantities considered to be constant. Fig. 1 summarizes the coupling interactions so far described.

2.2. Extended principle of virtual displacements and condensed notation

As stated in [9], piezoelectricity is based on a quasi-static approximation [1]. That assumption has been retained in the present work. The extended form of classical principle of virtual displacements (PVD) extended to PVD takes the following form [2]:

$$\int_V (\sigma_{ij}\delta\varepsilon_{ij} - \eta\delta\theta - D_l\delta E_l - B_l\delta H_l)\,dV = \delta L_e - \delta L_{in}, \tag{3}$$

where V is the plate volume, L_e and L_i are the work made by external and inertial loads, respectively, and δ is the variational symbol. In the case of applied electro-mechanical loading on a surface Ω, the virtual variation of the external work can be expressed as

$$\delta L_e = \int_\Omega (\bar{t}_i\delta u_i - \overline{Q}\delta\phi)\,d\Omega, \tag{4}$$

where $\bar{t}_i$ is the mechanical loading in j-direction (pressure); u_i is the displacement component in j-direction; $\overline{Q}$ is the charge density on the plate surface; ϕ is the electric potential.

Moreover, the expression for the virtual variation of the inertial load is

$$\delta L_i = \int_V \rho\ddot{u}_i\delta u_i\,dV, \tag{5}$$

where the dot denotes differentiation with respect to time.

For the purpose of condensed implementation, it has some advantages to replace indices with vectors. The following multifield arrays/vectors are introduced:

$$\boldsymbol{\mathcal{S}}^T = \{\sigma_{11}\ \sigma_{22}\ \sigma_{12}\ -D_1\ -D_2\ -B_1\ -B_2\ -\eta\ \sigma_{33}\ \sigma_{13}\ \sigma_{23}\ -D_3\ -B_3\}, \tag{6}$$

$$\boldsymbol{\mathcal{E}}^T = \{\varepsilon_{11}\ \varepsilon_{22}\ \varepsilon_{12}\ E_1\ E_2\ H_1\ H_2\ \theta\ \varepsilon_{33}\ \varepsilon_{13}\ \varepsilon_{23}\ E_3\ H_3\}. \tag{7}$$

$\boldsymbol{\mathcal{S}}$ is the vector of extensive variables while $\boldsymbol{\mathcal{E}}$ is the vector of intensive ones (bold letters denote arrays and ε_{ij} components in vectorial notation correspond to $2\varepsilon_{ij}$ components in tensorial notation, when $i\neq j$).

Note that dealing with plates, subscript "3" indicates the through-the-thickness z-direction while subscripts "1" and "2" are for the two in-plane directions. Non-mechanical quantities

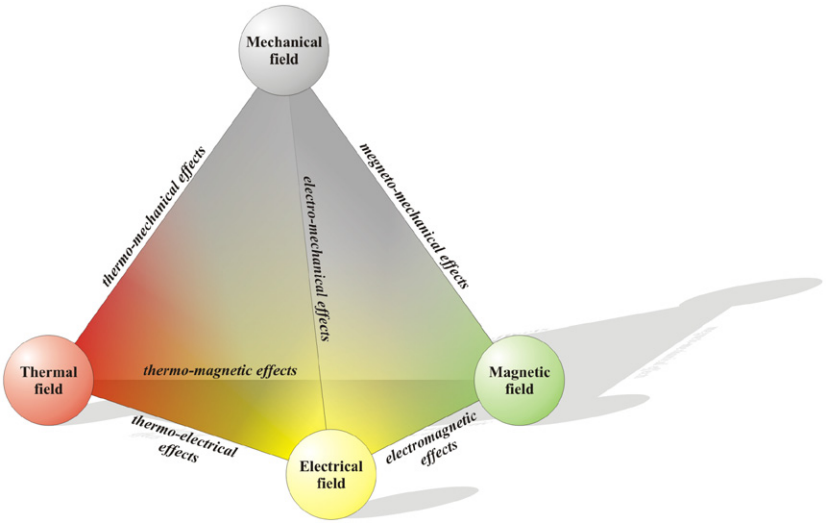

Fig. 1. Interaction processes between the mechanical, thermal, electrical, and magnetic fields.

appear under negative sign in vector $\mathcal{S}$ and this is due to the fact that non-mechanical quantities are negative in Eq. (1).

By using the two introduced vectors, the PVD statement takes the following "condensed" or "compact" form:

$$\int_V (\delta \boldsymbol{\mathcal{E}}_G^T \boldsymbol{\mathcal{S}}_H)\, dV = \delta L_e - \delta L_{in}, \tag{8}$$

where subscripts "G" and "H" indicate variables obtained by geometrical relations and by constitutive/Hooke's relations, respectively. For multilayered structures, the volume integral has to be intended as

$$\int_V (\cdots)\, dV = \sum_{k=1}^{N_l} \int_{\Omega_k} \int_{h_k} (\cdots)\, d\Omega_k\, dz, \tag{9}$$

where Ω_k is the layer middle surface, h_k denotes the k-layer thickness domain and N_l indicates the number of layers.

For convenience, the PVD in Eq. (8) can also be written in the following form:

$$\int_V (\delta \boldsymbol{\varepsilon}_{pG}^T \boldsymbol{\sigma}_{pH} + \delta \boldsymbol{\varepsilon}_{nG}^T \boldsymbol{\sigma}_{nH} - \delta \boldsymbol{H}_{pG}^T \boldsymbol{B}_{pH} - \delta H_{nG} B_{nH} - \delta \boldsymbol{E}_{pG}^T \boldsymbol{D}_{pH} - \delta E_{nG} D_{nH} - \delta \theta_G \eta_H)\, dV = \delta L_e - \delta L_{in}, \tag{10}$$

where notation already used in previous authors' work is referred to subscript "p" denotes in-plane unknowns and subscript "n" denotes out-of-plane unknowns.

2.3. Particular cases

The virtual variations in the previous four-fields form of PVD are six δu_1, δu_2, δu_3, $\delta\phi$, $\delta\varphi$, $\delta\theta$; where $\delta\varphi$ indicate the variations of magnetic potential.[1] In general, a virtual variation can be considered alone or can be coupled with the others. A few examples of variational statements for different case of coupling are considered in the following.

PVD-1: *Pure mechanical case*. If only virtual variations of displacements δu_1, δu_2, δu_3 are considered, Eq. (3) is reduced to

$$\int_V (\delta \boldsymbol{\varepsilon}_{pG}^T \boldsymbol{\sigma}_{pH} + \delta \boldsymbol{\varepsilon}_{nG}^T \boldsymbol{\sigma}_{nH})\, dV = \delta L_e - \delta L_{in}. \tag{11}$$

That is a pure mechanical problem is described.

[1] To be noticed that δu_1, δu_2, δu_3 come from the strain $\delta\varepsilon$, $\delta\phi$ from δE and $\delta\varphi$ from δH.

PVD-2: *Coupled thermo-mechanical case*. By adding the variation of temperature δu_1, δu_2, δu_3, $\delta\theta$, Eq. (3) becomes

$$\int_V (\delta \boldsymbol{\varepsilon}_{pG}^T \boldsymbol{\sigma}_{pH} + \delta \boldsymbol{\varepsilon}_{nG}^T \boldsymbol{\sigma}_{nH} - \delta\theta_G \eta_H)\, dV = \delta L_e - \delta L_{in}. \tag{12}$$

That is a coupled thermo-mechanical problem is described.

PVD-3: *Partially coupled thermo-mechanical case*. Saying that thermal field is partially coupled with mechanical field, means that the extensive variable concerning thermal field (η) is not considered in constitutive relations. The thermal field impacts the system under the form of thermal stresses σ_θ and thermal load vector. The advantage of using a partially coupled system lies in the reduction of the number of system degrees of freedoms. The disadvantage is that the thermal effect due to strain is neglected and the temperature must be known in any point of the considered continuum. Corresponding Eq. (3) is

$$\int (\delta \boldsymbol{\varepsilon}_{pG}^T (\boldsymbol{\sigma}_{pH} - \boldsymbol{\sigma}_{p\theta}) + \delta \boldsymbol{\varepsilon}_{nG}^T (\boldsymbol{\sigma}_{nH} - \boldsymbol{\sigma}_{n\theta}))\, dV = \delta L_e - \delta L_{in}. \tag{13}$$

PVD-4: *Coupled electro-mechanical case*. The considered virtual variations are δu_1, δu_2, δu_3, $\delta\phi$ and the PVD reduces to

$$\int_V (\delta \boldsymbol{\varepsilon}_{pG}^T \boldsymbol{\sigma}_{pH} + \delta \boldsymbol{\varepsilon}_{nG}^T \boldsymbol{\sigma}_{nH} - \delta \boldsymbol{E}_{pG}^T \boldsymbol{D}_{pH} - \delta E_{nG} D_{nH})\, dV = \delta L_e - \delta L_{in}. \tag{14}$$

PVD-5: *Coupled magneto-mechanical case*. The considered virtual variations are δu_1, δu_2, δu_3, $\delta\varphi$ and the PVD reduces to

$$\int_V (\delta \boldsymbol{\varepsilon}_{pG}^T \boldsymbol{\sigma}_{pH} + \delta \boldsymbol{\varepsilon}_{nG}^T \boldsymbol{\sigma}_{nH} - \delta \boldsymbol{H}_{pG}^T \boldsymbol{B}_{pH} - \delta H_{nG} B_{nH})\, dV = \delta L_e - \delta L_{in}. \tag{15}$$

PVD-6: *Coupled magneto-electro-mechanical case*. The considered virtual variations are δu_1, δu_2, δu_3, $\delta\phi$, $\delta\varphi$ and the PVD statement is

$$\int_V (\delta \boldsymbol{\varepsilon}_{pG}^T \boldsymbol{\sigma}_{pH} + \delta \boldsymbol{\varepsilon}_{nG}^T \boldsymbol{\sigma}_{nH} - \delta \boldsymbol{H}_{pG}^T \boldsymbol{B}_{pH} - \delta H_{nG} B_{nH} - \delta \boldsymbol{E}_{pG}^T \boldsymbol{D}_{pH} - \delta E_{nG} D_{nH})\, dV = \delta L_e - \delta L_{in}.$$

3. FE equations in terms of "fundamental nuclei"

In the context of the so-called axiomatic approaches where displacements or, more in general, stress field, thermal, electrical or magnetic variables are postulated in the thickness plate z-direction, two-dimensional plate elements are usually

constructed according to the following four steps.

(I) Material behavior is assigned, i.e. constitutive relations are given (see Section. 2.1).
(II) Geometrical relations (e.g. strain–displacement relations are assumed in the mechanical case).

$$\boldsymbol{H}^k=\begin{pmatrix} C_{11}^k & C_{12}^k & C_{16}^k & 0 & 0 & 0 & 0 & -\lambda_1^k & C_{13}^k & 0 & 0 & -e_{31}^k & -q_{31}^k \\ C_{12}^k & C_{22}^k & C_{26}^k & 0 & 0 & 0 & 0 & -\lambda_2^k & C_{23}^k & 0 & 0 & -e_{32}^k & -q_{32}^k \\ C_{16}^k & C_{26}^k & C_{66}^k & 0 & 0 & 0 & 0 & 0 & C_{36}^k & 0 & 0 & -e_{36}^k & -q_{36}^k \\ 0 & 0 & 0 & -\varepsilon_{11}^k & -\varepsilon_{12}^k & -d_{11}^k & -d_{12}^k & 0 & 0 & -e_{15}^k & -e_{14}^k & 0 & 0 \\ 0 & 0 & 0 & -\varepsilon_{12}^k & -\varepsilon_{22}^k & -d_{12}^k & -d_{22}^k & 0 & 0 & -e_{25}^k & -e_{24}^k & 0 & 0 \\ 0 & 0 & 0 & -d_{11}^k & d_{12}^k & -\mu_{11}^k & -\mu_{12}^k & 0 & 0 & -q_{15}^k & -q_{14}^k & 0 & 0 \\ 0 & 0 & 0 & -d_{12}^k & d_{22}^k & -\mu_{12}^k & -\mu_{22}^k & 0 & 0 & -q_{25}^k & -q_{24}^k & 0 & 0 \\ -\lambda_1^k & -\lambda_2^k & 0 & 0 & 0 & 0 & 0 & -\left(\frac{\rho C}{\theta_{ref}}\right)^k & -\lambda_3^k & 0 & 0 & -p_3^k & -r_3^k \\ C_{13}^k & C_{23}^k & C_{36}^k & 0 & 0 & 0 & 0 & -\lambda_3^k & C_{33}^k & 0 & 0 & -e_{33}^k & -q_{33}^k \\ 0 & 0 & 0 & -e_{15}^k & -e_{25}^k & -q_{15}^k & -q_{25}^k & 0 & 0 & C_{55}^k & C_{45}^k & 0 & 0 \\ 0 & 0 & 0 & -e_{14}^k & -e_{24}^k & -q_{14}^k & -q_{24}^k & 0 & 0 & C_{45}^k & C_{44}^k & 0 & 0 \\ -e_{31}^k & -e_{32}^k & -e_{36}^k & 0 & 0 & 0 & 0 & -p_3^k & -e_{33}^k & 0 & 0 & -\varepsilon_{33}^k & -d_{33}^k \\ -q_{31}^k & -q_{32}^k & -q_{36}^k & 0 & 0 & 0 & 0 & -r_3^k & -q_{33}^k & 0 & 0 & -d_{33}^k & -\mu_{33}^k \end{pmatrix}. \tag{20}$$

(III) Displacement, stress distribution, thermal, electrical or magnetic variables in the thickness plate z-direction are *postulated* by referring to a certain set of base functions.
(IV) An appropriate variational statement is used to establish FE matrices which are variationally consistent with the hypotheses introduced at points (I)–(III).

3.1. Geometrical and constitutive equation in condensed forms

$\boldsymbol{U}^k$ denotes the vector containing primary unknowns of the problem. Superscripts k and T indicate the k-th layer of the plate and the array transposition, respectively. A suitable choice for PVD application is

$$\boldsymbol{U}^{kT}=\{u_1^k\ u_2^k\ u_3^k\ \phi^k\ \varphi^k\ \theta^k\}. \tag{16}$$

The intensive variables $\boldsymbol{\mathcal{E}}^k$ are linearly related to the unknowns $\boldsymbol{U}^k$ according to the following geometrical relations:

$$\boldsymbol{\mathcal{E}}_G^k=\boldsymbol{D}\boldsymbol{U}^k, \tag{17}$$

where $\boldsymbol{D}$ denotes the following differential operator:

$$\boldsymbol{D}=\begin{pmatrix} \partial_x & 0 & 0 & 0 & 0 & 0 \\ 0 & \partial_y & 0 & 0 & 0 & 0 \\ \partial_y & \partial_x & 0 & 0 & 0 & 0 \\ 0 & 0 & 0 & -\partial_x & 0 & 0 \\ 0 & 0 & 0 & -\partial_y & 0 & 0 \\ 0 & 0 & 0 & 0 & -\partial_x & 0 \\ 0 & 0 & 0 & 0 & -\partial_y & 0 \\ 0 & 0 & 0 & 0 & 0 & 1 \\ 0 & 0 & \partial_z & 0 & 0 & 0 \\ \partial_z & 0 & \partial_x & 0 & 0 & 0 \\ 0 & \partial_z & \partial_y & 0 & 0 & 0 \\ 0 & 0 & 0 & -\partial_z & 0 & 0 \\ 0 & 0 & 0 & 0 & -\partial_z & 0 \end{pmatrix}. \tag{18}$$

Multilayered plates constituted by orthotropic layers (lamina) are treated in this work. The lamina are considered to be homogeneous and to operate in the linear elastic range. Once rotated in the laminate reference system and considering the four-field linear coupling, constitutive coefficient can be organized in matrix $\boldsymbol{H}^k$:

$$\boldsymbol{\mathcal{S}}_H^k=\boldsymbol{H}^k\boldsymbol{\mathcal{E}}_G^k, \tag{19}$$

where

3.2. Through-the-thickness assumptions for primary variables via CUF

In the framework of the CUF [10], the primary unknowns are assumed by using a generalized expansion:

$$\boldsymbol{U}^k(x,y,z)=F_\tau(z)\boldsymbol{U}_\tau^k(x,y),\quad \tau=0,1,\ldots,N, \tag{21}$$

while for virtual variations:

$$\delta\boldsymbol{U}^k(x,y,z)=F_s(z)\delta\boldsymbol{U}_s^k(x,y),\quad s=0,1,\ldots,N. \tag{22}$$

The repeated indexes are summed over their ranges. The polynomials $F_\tau(z)$ constitute a set of independent functions. Such base is arbitrarily chosen: power of z, Lagrange polynomials or a combination of Legendre polynomials can be considered. N denotes the order of the introduced expansion. Note that the variables concerning displacements, electrical potential, magnetic potential and temperature are included in vector $\boldsymbol{U}^k$.

It is understood that, by the arbitrary choice of the thickness expansion, the same computational code can address (by the same scheme) a complete family of FEs, with different descriptions for primary unknowns along the thickness of the structure. Meanwhile, in the developed code, the order of the expansion along the thickness of the plate is taken as a free parameter of the finite element and it can be changed ranging from 1 up to 4.

A global assumption for the unknowns is considered along the thickness of the plate (i.e. a Taylor expansion) in ESL models, while in a LW model the expansion is made for each layer separately and then interlaminar continuity conditions are enforced by the assembly procedure. The latter generally leads to more accurate results but the number of the nodal degrees of freedom increases with the number of the layers, leading to higher computational cost.

For a LW theory the thickness functions are defined by

$$F_t=\frac{P_0+P_1}{2},\quad F_b=\frac{P_0-P_1}{2},\quad F_r=P_r-P_{r-2},\quad r=2,\ldots,N, \tag{23}$$

where $P_i=P_i(\zeta_k)$ is the *Legendre* polynomial of i-th order defined in the domain $-1\le\zeta_k\le 1$. The chosen thickness functions have

the following interesting properties:

$$\zeta_k = \begin{cases} 1: & F_t = 1, \quad F_b = 0, \quad F_r = 0, \\ -1: & F_t = 0, \quad F_b = 1, \quad F_r = 0. \end{cases} \tag{24}$$

The generalized assumptions for the primary unknowns of the k-th layer in Eqs. (21), (22) can be stated as

$$\boldsymbol{U}^k(x,y,z) = F_b(z)\boldsymbol{U}_b^k(x,y) + F_r(z)\boldsymbol{U}_r^k(x,y) + F_t(z)\boldsymbol{U}_t^k(x,y) = F_\tau \boldsymbol{U}_\tau^k, \tag{25}$$

$$\delta\boldsymbol{U}^k(x,y,z) = F_b(z)\delta\boldsymbol{U}_b^k(x,y) + F_r(z)\delta\boldsymbol{U}_r^k(x,y) + F_t(z)\delta\boldsymbol{U}_t^k(x,y) = F_s\delta\boldsymbol{U}_s^k, \tag{26}$$

with $r=2,\ldots,N$.

The variables $\boldsymbol{U}_b$ and $\boldsymbol{U}_t$ are the actual primary unknowns at the bottom and the top surfaces of the layer and the interlaminar continuity can be easily imposed:

$$\boldsymbol{U}_t^k = \boldsymbol{U}_b^{(k+1)} \quad \text{with } k = 1,\ldots,N_l-1. \tag{27}$$

Acronyms are used for the implemented plate elements: LD1, LD2, LD3, LD4, where L states that a Layer-Wise description is employed and D indicates that classical approach based on PVD is used; 1–4 denotes the order of the expansion introduced for the field variables in each layer (from first to fourth-order). ED1, ED2, ED3, ED4 are used to denote correspondent equivalent-single-layer description based on Taylor expansion.

3.3. Finite element discretization

In case of FE implementation, unknowns and virtual variations can be expressed in terms of their nodal values, via the shape functions N_i:

$$\boldsymbol{U}_\tau^k(x,y) = N_i(x,y)\boldsymbol{Q}_{\tau i}^k, \quad i = 1,2,\ldots,N_n, \tag{28}$$

$$\delta\boldsymbol{U}_s^k(x,y) = N_j(x,y)\delta\boldsymbol{Q}_{sj}^k, \quad j = 1,2,\ldots,N_n, \tag{29}$$

where N_n denotes the number of nodes of the considered finite element and $\boldsymbol{Q}_{\tau i}^k$ is the vector of the nodal values of the primary unknowns:

$$\boldsymbol{Q}_{\tau i}^{kT} = \{Q_{u_1\tau i}^k \;\; Q_{u_2\tau i}^k \;\; Q_{u_3\tau i}^k \;\; Q_{\phi\tau i}^k \;\; Q_{\varphi\tau i}^k \;\; Q_{\theta\tau i}^k\}. \tag{30}$$

Substituting Eqs. (28), (29), in Eqs. (21), (22) the final expression of primary unknowns can be obtained:

$$\boldsymbol{U}^k(x,y,z) = F_\tau N_i \boldsymbol{Q}_{\tau i}^k. \tag{31}$$

3.4. Fundamental nucleus and FE matrices

Substituting Eqs. (17), (19), (21) and (28) in the variational statement of Eq. (8) leads to a set of equilibrium equations which can be formally put in the following compact form:

$$\delta\boldsymbol{Q}_{sj}^k : \boldsymbol{M}^{k\tau sij}\ddot{\boldsymbol{Q}}_{\tau i}^k + \boldsymbol{K}^{k\tau sij}\boldsymbol{Q}_{\tau i}^k = \boldsymbol{P}_{sj}^k, \tag{32}$$

where $\boldsymbol{P}^k$ is the vector of external loads. The related boundary conditions can be expressed by $\overline{\boldsymbol{Q}}^k$.

The number of obtained equations coincides with the number of introduced variables: τ and s vary from 0 to N, i and j vary from 1 to N_n and k ranges from 1 to N_l. Matrix $\boldsymbol{K}^{k\tau sij}$ is the so-called fundamental nucleus. In this case it is a 6×6 array and it provides the information to build the stiffness matrix. Matrix $\boldsymbol{M}^{k\tau sij}$ represents the fundamental nucleus related to the mass matrix.

Fundamental nuclei related to PVD-1−PVD-6 can be obtained as particular cases of Eq. (32). More details can be found in a DIASP internal report [11].

Whatever is the considered variational statement, starting from fundamental nucleus, for a given discretization, mass matrix $\boldsymbol{M}$ and stiffness matrix $\boldsymbol{K}$ can be calculated by numerical integration and the assembly procedure. These two matrices are representative of inertial and Gibbs free energy contribution, respectively. It should be emphasized that the stiffness matrix, regardless its name, contains information pertaining to all the considered fields and not only to the mechanical field. On the contrary, the mass matrix only concerns the mechanical field. In fact, mass apart, there are not other physical quantity related to the second time derivative of primary unknowns when defining the kinetic energy.

The stiffness matrix is symmetric due to the symmetric nature of the matrix products that form the variational statement lead to the fundamental nucleus. In addition, $\boldsymbol{K}$ is positive definite in the pure mechanical case, where only non-negative energetic contributions are admitted. One consequence of coupling the non-mechanical fields to the mechanical field is that the stiffness matrix becomes no longer positive defined: the non-mechanical fields imply a negative amount of mechanical energy due to negative coefficients along the diagonal of the constitutive matrix in Eq. (20) (such negative coefficients cause negative numbers on the diagonal of $\boldsymbol{K}$). The amount of energy subtracted from the mechanical field results as distributed among the coupled fields under the form of thermal, electric or magnetic energy, leaving unchanged the total amount of energy. Consequently, the efficient positive definite matrix solution algorithms used in pure mechanical analysis cannot be adopted in multifield problems. That is a coupled problem is more time consuming to solve than a pure structural problem of the same size.

The undamped dynamic problem can be written in terms of the following ordinary differential equations system:

$$\boldsymbol{M}\ddot{\boldsymbol{Q}} + \boldsymbol{K}\boldsymbol{Q} = \boldsymbol{F}, \tag{33}$$

where $\boldsymbol{Q}$ is the vector of nodal primary unknowns; $\ddot{\boldsymbol{Q}}$ is the vector of accelerations; $\boldsymbol{F}$ is the vector of nodal loads.

Moreover, the i-th natural frequency of the system ω_i can be calculated by solving the generalized eigenvalues problem:

$$(-\omega_i^2\boldsymbol{M} + \boldsymbol{K})\boldsymbol{a_i} = \boldsymbol{0}, \tag{34}$$

where $\boldsymbol{a_i}$ is the i-th eigenvector.

If a static analysis is required, the system to solve is the following:

$$\boldsymbol{K}\boldsymbol{Q} = \boldsymbol{F}. \tag{35}$$

Such system can be solved by taking into account the boundary conditions $\overline{\boldsymbol{Q}}_\Gamma^k$, which are related to the various fields addressed in the analysis.

4. Numerical results

This section shows several numerical results employed to assess the developed FEs for magneto-electro-thermo-elastic plate problems. Various "sample" problems related to interaction of various fields have been solved. These are quoted in different subsections. Comparisons between present numerical results and the corresponding closed form approximated or 3D exact solutions available in literature are provided. Presented FEM results are often denoted as "MUL2 results". Reduced integration techniques have been preserved in MUL2 as done in [5,8,12,13], to overcome locking phenomena. Moreover, thickness locking correction via reduction of the constitutive relations has been employed as illustrated in [14]. Regular meshes have been used everywhere.

Table 1
Material properties of the aluminium alloy Al 2024-T6.

	E (GPa)	G (GPa)	ν_{12} (−)	ρ (kg/m^3)
Al 2024-T6	73	27.239	0.34	2800

Table 2
Pure mechanical problem.

Frequency number	Analytical	FEM (mesh)		
		(3 × 3)	(6 × 6)	(9 × 9)
1	6.0570	6.0701	6.0578	6.0572
2	15.134	15.563	15.163	15.140
3	15.134	15.563	15.163	15.140
4	24.202	24.968	24.254	24.212

Plate undamped dimensionless natural frequencies calculated for the pure mechanical case: convergence study of the Q9 ED4 finite element to the corresponding analytical solution—see Fig. 2.

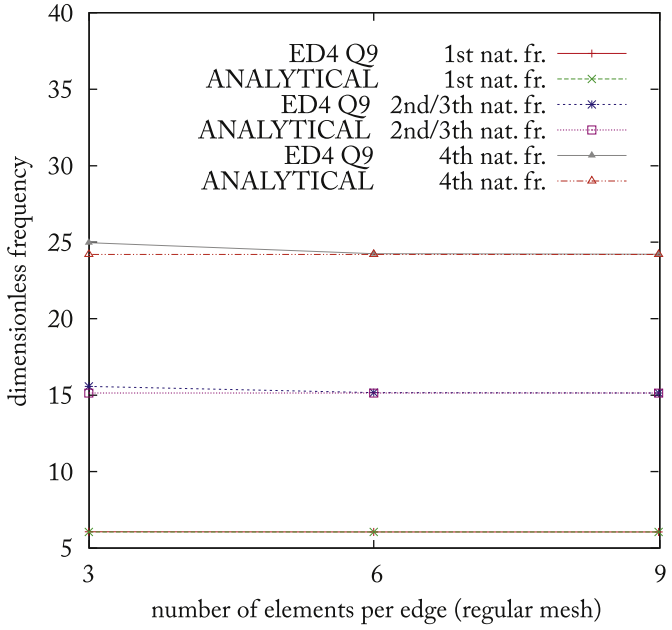

Fig. 2. Convergence study in Table 2 for the first three frequencies.

4.1. Pure mechanical problems

A simply supported square plate of aluminium alloy 2024-T6 is considered under PVD-1 analysis with a regular mesh of nine-nodes Quadrangular FEs (Q9). A regular mesh is a mesh with the same number of equally spaced elements along the two plate's directions. Material properties are those in Table 1. The plate thickness ratio is $a/h=0.01$ (where a is the plate side length and h is the thickness). A fourth order through-the-thickness expansion for primary variables is considered and the ESL theory is employed (ED4). Dimensionless undamped natural frequencies $\overline{\omega}=\omega\sqrt{a^4\rho/(h^2E)}$ (where ρ is the material density and E is Young's modulus) obtained by MUL2 are compared to the corresponding analytical results in Table 2 and Fig. 2 [14]. The first natural frequencies of the structure are calculated with reasonable accuracy even with very poor meshes of Q9 FEs (e.g. 3×3).

A convergence study for ED1 Q4 FEs is provided in Table 3 and Fig. 3, where results obtained in NASTRAN commercial code are listed as well. NASTRAN and MUL2 convergence properties are in good agreement. A 15×15 mesh of Q4 FEs would represent a good compromise between accuracy and computational effort.

Fig. 4 shows that the present formulation permits to detect the so-called thickness modes which are discarded by those classical theories which neglect trough-the-thickness strains.

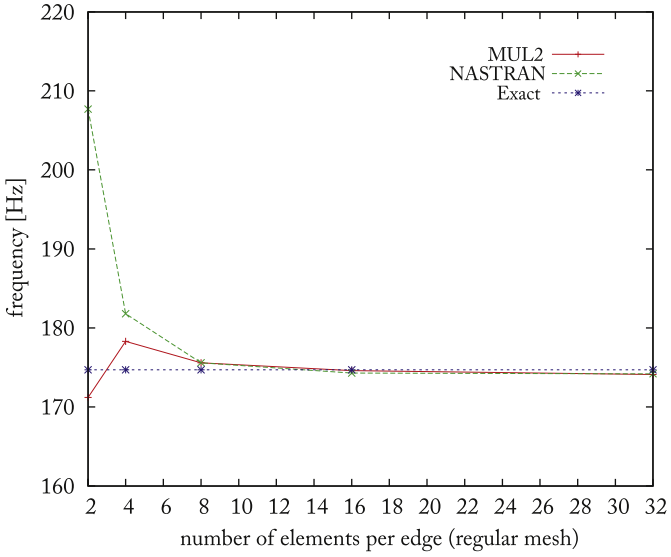

Fig. 3. Convergence study in Table 3.

Table 3
Pure mechanical problem.

Q9 uniform mesh size	Vibration mode number (M=MUL2/N=NASTRAN)							
	1 (M)	1 (N)	2 (M)	2 (N)	5 (M)	5 (N)	6 (M)	6 (N)
2 × 2	171.2	207.7	11 569.8	11 188.8	11 781.5		11781.5	
4 × 4	178.3	181.8	566.6	517.5	1858.7	1311.7	1858.7	1311.7
8 × 8	175.6	175.6	463.1	452.8	1022.2	965.2	1022.2	965.2
16 × 16	174.6	174.3	422.0	439.1	905.2	891.8	905.2	891.8
32 × 32	174.1	174.2	436.9	436.4	879.1	876.1	879.1	876.1
Exact sol.[a]	174.7	174.7	436.8	436.8	873.6	873.6	873.6	873.6

Convergence analysis of frequency [Hz] with mesh refinement for an isotropic, simply supported, square plate ($a=b=0.3$ m, $t=0.0032$ m, $E=210E$ 9 N/m^2, $\nu=0.3$ and $\rho=7860$ kg/m^3)—comparison between MUL2 results (LD1 FEs) and Nastran results.

[a] Based on thin (shear-rigid) plate theory.

4.2. Thermo-mechanical problems

Results of thermo-mechanical static analysis of multilayered anisotropic plates related to PVD-3 applications are discussed. The problem proposed by Bhaskar and Varadan [15] is considered. Numerical results are presented for the bending of a $(0^\circ/90^\circ/0^\circ)$ square (square $a=b$) laminate plate due to the temperature field given by

$$\theta = \overline{\theta}(2z/h)\sin\left(\frac{\pi x}{a}\right)\sin\left(\frac{\pi y}{b}\right), \tag{36}$$

where h is the total thickness of the laminate. The following material properties, typical of high-modulus graphite/epoxy, are assumed: $E_L/E_T=25$; $G_{LT}/E_T=0.5$; $G_{TT}/E_T=0.2$; $\nu_{LT}/\nu_{TT}=0.25$; $\alpha_T/\alpha_L=1125$, where ν is Poisson's coefficient, α is the coefficient of thermal expansion. L and T refer to directions parallel and perpendicular, respectively, to the fibers.

Note that the distribution of temperature along the thickness, for given thermal boundary conditions at the top and at the bottom surfaces, can be obtained by solution of the heat conduction equation [16,17]. However, only simple linear antisymmetric (with respect to z) thermal variation is considered as this would lead to bending (without stretching) of a symmetric laminate and would be adequate to bring out the importance of non-classical influences such as shear deformation and thickness stretch.

The deflections and stresses are presented in terms of the following dimensionless parameters:

$$\tilde{u}_3 = \frac{u_3}{h\alpha_L\overline{\theta}S^2}, \quad (\tilde{u}_1,\tilde{u}_2) = \frac{(u_1,u_2)}{h\alpha_L\overline{\theta}S}, \quad \tilde{\sigma}_{ij} = \frac{\sigma_{ij}}{E_T\alpha_L\overline{\theta}},$$

with $S=a/h$.

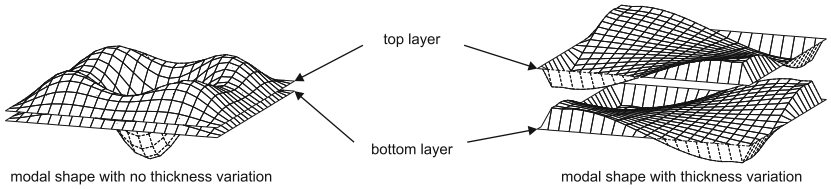

Fig. 4. Two modal shapes of a generic plate: the right picture emphasizes the capability of present formulation to capture the through-the-thickness modes—Q4 ED1 FEs.

Table 4
Thermo-mechanical problem: thermal response of square plate, comparison between present results and those in [15].

S	Sol.	$\tilde{u}_1\left(\mp\frac{h}{2}\right)$	$\tilde{u}_2\left(\mp\frac{h}{2}\right)$	$\tilde{u}_3\left(\mp\frac{h}{2}\right)$	$\tilde{\sigma}_{11}\left(\pm\frac{h}{2}\right)$	$\tilde{\sigma}_{22}\left(\mp\frac{h}{2}\right)$	$\tilde{\sigma}_{12}\left(\mp\frac{h}{2}\right)$
2	3D [15]	±20.04	±151.4	96.79	±1390	±635.4	±269.3
2	FEM	±12.88	±162.4	90.38	±672.3	±711.3	±281.5
4	3D [15]	±18.11	±81.83	42.69	±1183	±856.1	±157.0
4	FEM	±16.51	±86.08	41.82	±916.0	±960.2	±164.9
10	3D [15]	±16.61	±31.95	17.39	±1026	±1014	±76.29
10	FEM	±17.31	±33.47	17.84	±945.3	±1134	±81.65
20	3D [15]	±16.17	±20.34	12.12	±982.0	±1051	±57.35
20	FEM	±17.29	±21.59	12.82	±936.4	±1173	±62.55
50	3D [15]	±16.02	±16.71	10.50	±967.5	±1063	±51.41
50	FEM	±17.26	±17.92	11.27	±931.7	±1186	±56.55
100	3D [15]	±16.00	±16.17	10.26	±965.4	±1065	±50.53
100	FEM	±17.25	±17.40	11.05	±930.1	±1187	±55.65
CLT	EX. [15]	±15.99	±15.99	10.18	±964.6	±1065	±50.24

z values are given in parentheses; (x, y) values are: $(a/2, a/2)$ for $\tilde{u}_3$, $\tilde{\sigma}_{11}$ and $\tilde{\sigma}_{22}$; $(0,a/2)$ for $\tilde{u}_1$; $(a/2,0)$ for $\tilde{u}_2$ and $(0,0)$ for $\tilde{\sigma}_{12}$—a regular 6×6 mesh of Q9 LD1 FEs is employed.

Table 5
As Table 4, with the difference that LD4 FEs are employed.

S	Sol.	$\tilde{u}_1\left(\mp\frac{h}{2}\right)$	$\tilde{u}_2\left(\mp\frac{h}{2}\right)$	$\tilde{u}_3\left(\mp\frac{h}{2}\right)$	$\tilde{\sigma}_{11}\left(\pm\frac{h}{2}\right)$	$\tilde{\sigma}_{22}\left(\mp\frac{h}{2}\right)$	$\tilde{\sigma}_{12}\left(\mp\frac{h}{2}\right)$
2	3D [15]	±20.04	±151.4	96.79	±1390	±635.4	±269.3
2	FEM	±20.09	±151.4	96.74	±1432	±624.2	±275.3
4	3D [15]	±18.11	±81.83	42.69	±1183	±856.1	±157.0
4	FEM	±18.16	±81.82	42.68	±1220	±850.2	±160.5
10	3D [15]	±16.61	±31.95	17.39	±1026	±1014	±76.29
10	FEM	±16.66	±31.91	17.39	±1059	±1012	±78.05
20	3D [15]	±16.17	±20.34	12.12	±982.0	±1051	±57.35
20	FEM	±16.21	±20.29	12.12	±1013	±1050	±58.69
50	3D [15]	±16.02	±16.71	10.50	±967.5	±1063	±51.41
50	FEM	±16.05	±16.68	10.50	±997.4	±1061	±52.58
100	3D [15]	±16.00	±16.17	10.26	±965.4	±1065	±50.53
100	FEM	±16.01	±16.16	10.26	±994.3	±1063	±51.66
CLT	EX. [15]	±15.99	±15.99	10.18	±964.6	±1065	±50.24

A comparison between the 3D exact solution of the above described problem [15] and the present MUL2 results is given in Tables 4 and 5. A 6×6 mesh of Q9 FEs is employed. Two different kinematic are considered: Table 4 shows LD1 FEM results while Table 5 shows the values obtained with LD4 FEs. Results are free of thickness-locking and Poisson locking' as in [14]. LD4 FEM results are in excellent agreement with the exact solution both for displacement and for in-plane stresses, even though the employed mesh is not so refined.

Results of the convergence study for displacement u_1 and for in-plane stress σ_{11} can be found in Figs. 5 and 6. It can be noticed that FEM solutions converge to the 3D exact values [15] and that accurate results for displacements and in-plane stresses are obtained by Q9 FEs even with a poor mesh. It is confirmed that the convergence rate is higher for displacements than for stresses, see also [8,18].

As a further example a simply supported square aluminium plate is considered to investigate the "full" coupling between temperature and mechanical fields. To the authors' best knowledge no results are available on that topic. The reason of this absence lies on the fact that such a coupling is negligible for those materials which are normally employed in thermal structures. It is an application of PVD-2 statement. The analysis of a simple isotropic plate is proposed. Results are shown in dimensional form so that numbers can be judged by engineering sense. The mechanical properties are

$$E = 73\,\text{GPa}, \quad \nu = 0.3, \quad \alpha = 25\text{E}{-6}\,\text{K}^{-1}, \quad C = 897\,\text{J/kg K}, \quad \rho = 2800\,\text{kg/m}^3.$$

The plate dimensions are length and width $a = b = 10$ m, thickness $h = 1$ m. The plate has been loaded at the top face by the bi-sinusoidal pressure:

$$p = p_m \sin\left(\frac{\pi x}{a}\right) \sin\left(\frac{\pi y}{b}\right), \tag{37}$$

where the peak value is $p_m = 200$ MPa. A sketch can be seen in Fig. 7. A 6×6 mesh of LD4 Q9 elements is employed. The comparison between full thermal analysis and simple mechanical analysis is shown in Figs. 8–10 for the three displacements. It can be noted that there is not substantial difference in terms of

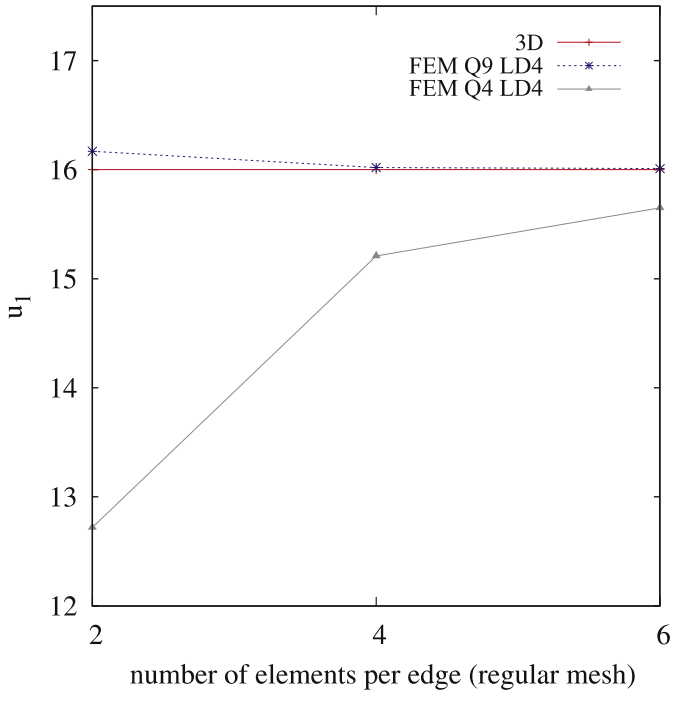

Fig. 5. Convergence study for displacement u_1.

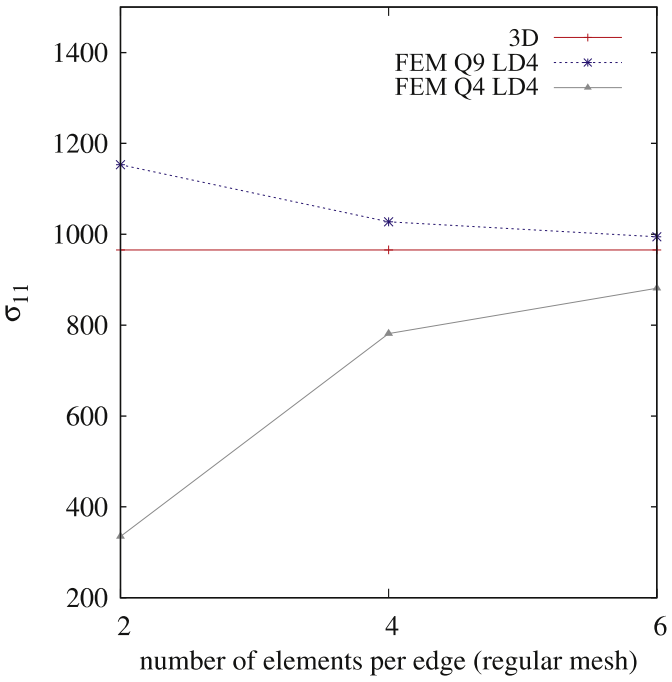

Fig. 6. Convergence study for stress σ_{11}.

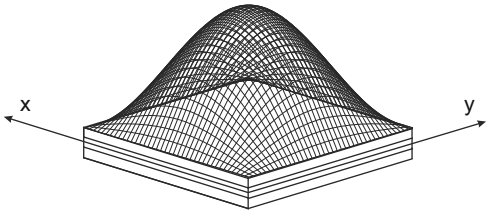

Fig. 7. Load and plate configuration.

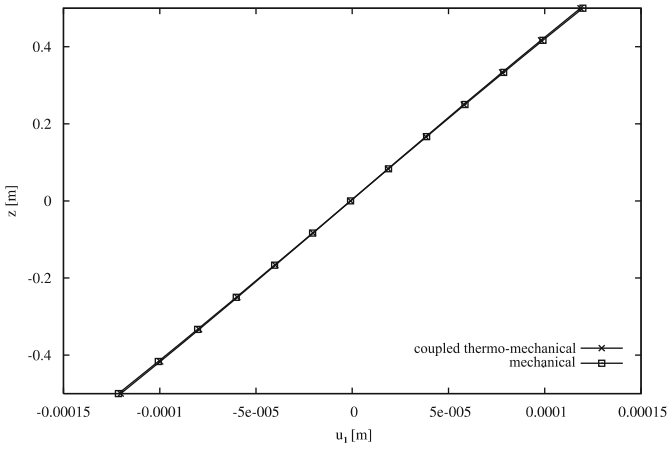

Fig. 8. Thermo-mechanical problem. $u_1(0,b/2)$, 6×6 mesh, LD4 Q9 elements—comparison between mechanical and coupled thermomechanical results.

in-plane displacements u_1 and u_2 (Figs. 8 and 9, respectively). A slight difference can be seen in Fig. 10 for displacement u_3. Anyway such distinction is still very small. The fact is that for a fully coupled thermo-mechanical analysis, only a small part of work is employed to modify the temperature of the plate. The u_3 displacement for this kind of analysis results to be smaller than the one obtained by a simple mechanical analysis because a part

of the work is used to develop the temperature variation. The same amount of work is subtracted from the work used to deform the plate. It can be seen that only a small part of work has been used to modify the temperature. In fact, the maximum value of thermal variation is 0.02 K. Normal stresses have been calculated successfully using both the analyses.

4.3. Electro-mechanical problems

In this section a few results of electro-mechanical analysis are compared with the exact solution provided by Heyliger [19]. The laminate considered is a [0/90] cross-ply composed of an elastic material with piezoelectric layers bonded to the upper and lower surfaces. The plate is square of side length a. The total thickness is h. The elastic layers have thickness of 0.4 h with the piezoelectric layer thicknesses of 0.1 h. The elastic material is modeled after a fiber-reinforced composite and has the properties $E_{11}=132.38$ (all in [GPa]), $E_{22}=10.756$, $E_{33}=10.756$, $G_{44}=3.606$, $G_{55}=5.654$, $G_{66}=5.654$, $\nu_{12}=0.24$, $\nu_{13}=0.24$, $\nu_{23}=0.49$, $\varepsilon_{11}/\varepsilon_0=3.5$, and $\varepsilon_{22}/\varepsilon_0=\varepsilon_{33}/\varepsilon_0=3.0$. The piezoelectric layers are modeled after PZT-4 and have the material properties $E_{11}=E_{22}=81.3$ (all in [GPa]), $E_{33}=64.5$, $G_{44}=G_{55}=25.6$, $G_{66}=30.6$, $\nu_{12}=0.329$, $\nu_{13}=\nu_{23}=0.432$, $e_{31}=e_{32}=-5.20$ (all in [C/m^2]), $e_{33}=15.08$, $e_{24}=e_{15}=12.72$, and $\varepsilon_{11}/\varepsilon_0=\varepsilon_{11}/\varepsilon_0=1475$, $\varepsilon_{33}/\varepsilon_0=1300$. The piezoelectric layer thicknesses are taken as 0.1 m.

Both applied double sinusoidal pressure loading and double sinusoidal surface potential are considered at the top plate surface: sensor and actuator configurations, respectively. See the two configurations in Fig. 11, where p_z indicates a pressure [N/m^2] and ϕ_t indicates the potential [V] imposed at the top face and $\hat{p}_z=\hat{\phi}_t=1$. The aspect ratio in both cases is $a/h=4$. For the

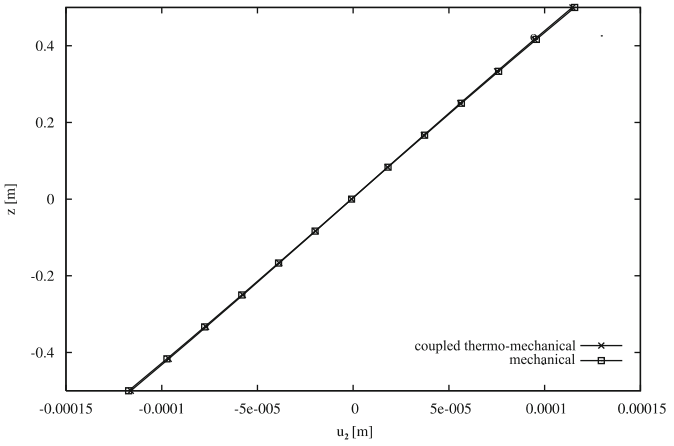

Fig. 9. Thermo-mechanical problem. $u_2(a/2,0)$, 6×6 mesh, LD4 Q9 elements—comparison between mechanical and coupled thermo-mechanical results.

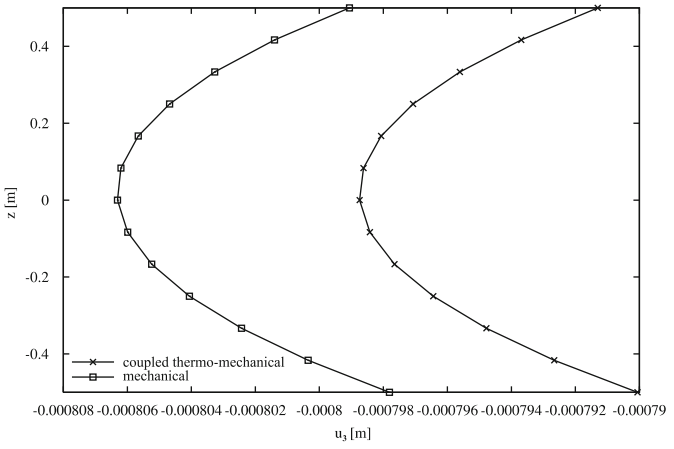

Fig. 10. Thermo-mechanical problem. $u_3(a/2,b/2)$, 6×6 mesh, LD4 Q9 elements—comparison between mechanical and coupled thermo-mechanical results.

Table 6
Electro-mechanical problem.

Sol.	$u_2\left(\frac{a}{2},0,\frac{h}{2}\right)$	$u_3\left(\frac{a}{2},\frac{a}{2},0\right)$	$\phi\left(\frac{a}{2},\frac{a}{2},0\right)$	$\sigma_{12}\left(0,0,\frac{h}{2}\right)$	$\sigma_{22}\left(\frac{a}{2},\frac{a}{2},\frac{h}{2}\right)$
3D [19]	−4.7549E−11	3.0027E−10	6.11E−3	−2.4776	6.5643
LD1	−4.6171E−11	2.9848E−10	6.0111E−3	−2.4946	6.8348
LD2	−4.7443E−11	2.9978E−10	6.1011E−3	−2.5255	6.2586
LD3	−4.7628E−11	3.0025E−10	6.1173E−3	−2.5332	6.2642
LD4	−4.7630E−11	3.0025E−10	6.1176E−3	−2.5332	6.2641
ED1	−2.4461E−11	1.8446E−10	2.6635E−3	−1.6585	3.2675
ED2	−3.1366E−11	2.0910E−10	6.2727E−3	−2.0879	1.1330
ED3	−4.5036E−11	2.8497E−10	5.8379E−3	−2.5116	1.3953
ED4	−4.7567E−11	2.8581E−10	6.1351E−3	−2.5286	1.8642

Results related to the sensor configuration; the mesh is 6×6 regular of Q9 FEs; displacements are in [m], the electric potential is in [V] and stresses are in [N/m^2].

Table 7
Electro-mechanical problem.

Sol.	$u_2\left(\frac{a}{2},0,\frac{h}{2}\right)$	$u_3\left(\frac{a}{2},\frac{a}{2},0\right)$	$\phi\left(\frac{a}{2},\frac{a}{2},0\right)$	$\sigma_{12}\left(0,0,\frac{h}{2}\right)$	$\sigma_{22}\left(\frac{a}{2},\frac{a}{2},\frac{h}{2}\right)$
3D [19]	−3.2764E−11	−1.4711E−11	4.476E−1	−1.4603	1.1181
LD1	−2.3764E−11	−1.6965E−11	4.4693E−1	−1.2983	3.4555
LD2	−2.2516E−11	−1.5490E−11	4.4805E−1	−1.2532	1.5853
LD3	−2.2602E−11	−1.5560E−11	4.4801E−1	−1.2765	1.4782
LD4	−2.2648E−11	−1.5580E−11	4.4801E−1	−1.2791	1.4598
ED1	−2.9655E−11	−1.5005E−11	4.4621E−1	−2.7358	4.5438
ED2	−1.9209E−11	−1.3684E−11	4.4879E−1	−1.2923	5.2010
ED3	−3.2936E−11	−3.6096E−11	4.4822E−1	−1.7342	10.967
ED4	−2.7908E−11	−3.3901E−11	4.4844E−1	−1.4429	11.580

Results related to the actuator configuration; the mesh is 6×6 regular of Q9 FEs; displacements are in [m], the electric potential is in [V] and stresses are in [N/m^2].

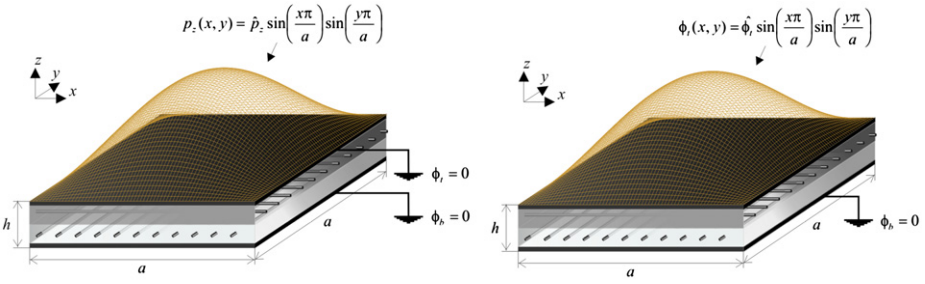

Fig. 11. On the left the plate in sensor configuration (applied pressure); on the right the plate in actuator configuration (applied potential).

applied pressure load, top and bottom laminate surfaces are fixed at zero potential. For the applied potential, these surfaces are stress free and the bottom surface is fixed to zero potential. A 6×6 regular mesh of Q9 FEs is employed. Results are in Tables 6 and 7 for the sensor and the actuator cases, respectively.

The following considerations on the obtained results can be done for both case studies: FEM results achieved by LW theory are in general more accurate with respect to those achieved by the ESL theory. For displacements, LW results obtained with a first order through-the-thickness expansion are more accurate than ESL results obtained with a fourth order expansion. Stress results provided by LW analysis are in good agreement with the exact solution, while the ESL theory can lead to significant errors. In fact, the ESL kinematic description, whatever is the order of expansion, cannot reproduce the plate-thickness zig-zag trend of primary unknowns at the layer interfaces [3]. This has a significant impact on the stresses which are calculated from strains, involving the displacement derivatives. Refining the mesh would not improve the ESL results since the problem is at the level of kinematic modeling. The way to enhance the solution is to use more advanced kinematic descriptions for the unknowns through-the-thickness of the plate. The LW description fully satisfies the zig-zag trend of quantities at the layer interfaces, even if a first order expansion is chosen (LD1). Increasing the order expansion improves the LW results, approaching the 3D exact solution.

In conclusion, it has been showed that results provided by LW FEs based on the PVD statement are very close to exact solutions for both piezoelectric sensor and actuator cases. Anyway, such a conclusion could not be extended to different plate problems or to results related to other variables evaluated in different points.

4.4. Electro-magneto-mechanical problems

This section shows some numerical results obtained for the PVD-6 case to assess the developed FEs for static magneto-electro-mechanical multilayered plate problems. Present FE analyses are compared with 3D exact solution by Pan [20]. Square plates which are loaded at the top layer surface and with simply supported edges are analyzed. Layered plates are build by using a combination of layers made of piezoelectric and magnetostrictive materials. The piezoelectric material consists of $BaTiO_3$ (called B for brevity) and the magnetostrictive one $CoFe_2O_4$ (called F for brevity). The physical properties of these two materials are given in Table 8 where C_{ij}, e_{ij}, q_{ij} are the stiffness, piezoelectric and piezomagnetic coefficients while ε_{ij} and μ_{ij} are the electric permittivity and the magnetic permeability, respectively.

The considered stacking sequences are B/F/B and F/B/F, the load is a bi-sinusoidal pressure of peak $1\,N/m^2$, applied at the top face; each layer has the same thickness $h_k=0.1$ m, plate length is $a=1$ m and all the quantities have been calculated with correspondence to the in-plane coordinate values: $x=0.75$ m and $y=0.25$ m, as done in the referenced article [20].

The employed mesh is regular 4×4 of Q9 FEs. LW and ESL results are here compared with the exact solution. Linear, parabolic, third and fourth order LW and ESL results are compared in Tables 9–12. Tables 9 and 10 collect results of mechanical electric and magnetic quantities, calculated for the B/F/B staking sequence; Tables 11 and 12 provide the same information in case of F/B/F staking sequence.

At this point it is important to underline that in the FEM analysis the plate is considered as sensor. As a consequence, electric and magnetic potentials are set to zero both at the top and at the bottom faces. Since such boundary condition is not imposed in the exact solution, FEM and exact potential values are not in agreement. Anyway, this discrepancy does not affect results related to other quantities.

Displacements calculated by ESL theory are often (but not always) close to the exact solution, but a high order through-the-thickness expansion is often required. With the LW approach good

Table 8
Properties of the materials employed in the Electro-magneto-mechanical problems.

Properties	$BaTiO_3$	$CoFe_2O_4$
C_{11} (GPa)	166	286
C_{22} (GPa)	166	286
C_{12} (GPa)	77	173
C_{13} (GPa)	78	170.5
C_{23} (GPa)	78	170.5
C_{33} (GPa)	162	269.5
C_{44} (GPa)	43	45.3
C_{55} (GPa)	43	45.3
C_{66} (GPa)	44.5	56.5
$\varepsilon_{11} \times 10^9$ ($C^2/(N\,m^2)$)	11.2	0.08
$\varepsilon_{22} \times 10^9$ ($C^2/(N\,m^2)$)	11.2	0.08
$\varepsilon_{33} \times 10^9$ ($C^2/(N\,m^2)$)	12.6	0.093
$\mu_{11} \times 10^6$ ($N\,s^2/C^2$)	5	−590
$\mu_{22} \times 10^6$ ($N\,s^2/C^2$)	5	−590
$\mu_{33} \times 10^6$ ($N\,s^2/C^2$)	10	157
e_{31} (C/m^2)	−4.4	0
e_{32} (C/m^2)	−4.4	0
e_{33} (C/m^2)	18.6	0
e_{24} (C/m^2)	11.6	0
e_{15} (C/m^2)	11.6	0
q_{31} ($N/(A\,m)$)	0	580.3
q_{32} ($N/(A\,m)$)	0	580.3
q_{33} ($N/(A\,m)$)	0	699.7
q_{24} ($N/(A\,m)$)	0	550
q_{15} ($N/(A\,m)$)	0	550

Table 9
Electro-magneto-mechanical problem.

	σ_{33} (Pa) Top face	σ_{13} (Pa) Center	u_1 (m) Bottom face	u_3 (m) Bottom face
3D [20]	0.5	-3.96×10^{-1}	-2.01×10^{-12}	5.4×10^{-12}
LD1	0.74	-4.14×10^{-1}	-2.02×10^{-12}	5.5×10^{-12}
LD2	0.57	-4.31×10^{-1}	-2.05×10^{-12}	5.6×10^{-12}
LD3	0.55	-4.24×10^{-1}	-2.05×10^{-12}	5.6×10^{-12}
LD4	0.51	-4.23×10^{-1}	-2.05×10^{-12}	5.6×10^{-12}
ED1	1.38	-1.94×10^{0}	-1.24×10^{-13}	5.7×10^{-12}
ED2	3.95	-3.04×10^{-1}	-1.50×10^{-13}	6.4×10^{-12}
ED3	2.96	-1.00×10^{0}	-1.44×10^{-13}	6.72×10^{-12}
ED4	9.18	-4.78×10^{-2}	-1.45×10^{-13}	6.82×10^{-12}

Comparison of various kinematics for the B/F/B plate: evaluation of transverse stresses and displacements. The mesh is regular 4×4 of Q9 FEs.

Table 10
Electro-magneto-mechanical problem.

	ϕ_{MAX} [V]	ψ_{MAX} (C/s)	σ_{11} (Pa) Top face	σ_{12} (Pa) Bottom face
3D [20]	1.54×10^{-3}	-2.61×10^{-6}	1.27	-5.77×10^{-1}
LD1	8.33×10^{-4}	-7.07×10^{-7}	1.43	-5.38×10^{-1}
LD2	8.39×10^{-4}	-7.15×10^{-7}	1.39	-5.47×10^{-1}
LD3	8.39×10^{-4}	-7.11×10^{-7}	1.38	-5.48×10^{-1}
LD4	8.39×10^{-4}	-7.12×10^{-7}	1.38	-5.48×10^{-1}
ED1	5.98×10^{-4}	-6.65×10^{-7}	2.67	-3.35×10^{-2}
ED2	1.01×10^{-3}	-8.22×10^{-7}	4.39	-3.06×10^{-2}
ED3	9.86×10^{-4}	-8.08×10^{-7}	5.76	-3.02×10^{-2}
ED4	9.97×10^{-4}	-1.01×10^{-6}	9.72	-2.65×10^{-2}

Comparison of various kinematics for the B/F/B plate: evaluation of in-plane stresses and electric and magnetic potentials. The mesh is regular 4×4 of Q9 FEs.

Table 11
Electro-magneto-mechanical problem.

	σ_{33} (Pa) Top face	σ_{13} (Pa) Center	u_1 (m) Bottom face	u_3 (m) Bottom face
3D [20]	0.5	-3.86×10^{-1}	-1.57×10^{-12}	4.38×10^{-12}
LD1	0.83	-3.97×10^{-1}	-1.55×10^{-12}	4.33×10^{-12}
LD2	0.53	-4.11×10^{-1}	-1.583×10^{-12}	4.40×10^{-12}
LD3	0.51	-4.06×10^{-1}	-1.584×10^{-12}	4.40×10^{-12}
LD4	0.51	-4.06×10^{-1}	-1.585×10^{-12}	4.40×10^{-12}
ED1	1.56	-1.25×10^{0}	-1.30×10^{-13}	4.00×10^{-12}
ED2	8.73	-3.22×10^{-1}	-1.57×10^{-13}	5.44×10^{-12}
ED3	3.91	-7.84×10^{-1}	-1.58×10^{-13}	5.56×10^{-12}
ED4	16.4	-1.95×10^{-1}	-1.59×10^{-13}	5.64×10^{-12}

Comparison of various kinematics for the F/B/F plate: evaluation of transverse stresses and displacements. The mesh is regular 4×4 of Q9 FEs.

Table 12
Electro-magneto-mechanical problem.

	ϕ_{MAX} (V)	ψ_{MAX} (C/s)	σ_{11} (Pa) Top face	σ_{12} (Pa) Bottom face
3D [20]	2.30×10^{-3}	-1.88×10^{-6}	1.33	-5.69×10^{-1}
LD1	5.54×10^{-4}	-1.63×10^{-7}	1.6	-5.49×10^{-1}
LD2	5.56×10^{-4}	-1.53×10^{-7}	1.44	-5.74×10^{-1}
LD3	5.58×10^{-4}	-1.55×10^{-7}	1.42	-5.74×10^{-1}
LD4	5.58×10^{-4}	-1.55×10^{-7}	1.42	-5.74×10^{-1}
ED1	4.48×10^{-4}	-3.00×10^{-6}	2.65	-4.81×10^{-2}
ED2	4.84×10^{-4}	-1.90×10^{-6}	8.26	-4.18×10^{-2}
ED3	5.62×10^{-4}	-1.73×10^{-6}	6.89	-4.21×10^{-2}
ED4	5.10×10^{-4}	-1.41×10^{-6}	15.9	-3.61×10^{-2}

Comparison of various kinematics for the F/B/F plate: evaluation of in-plane stresses and electric and magnetic potentials. The mesh is regular 4×4 of Q9 FEs.

results for displacement can be reached even without a high order through-the-thickness expansion. In general, best results for stresses are obtained by LW theory with high order through-the-thickness expansion, while ESL approach can lead to unreasonable numbers. More details and results can be found in another work devoted to interactions between the magnetic field and the others [21].

5. Conclusions

An advanced variable kinematic FE plate model, which is based on extended principle of virtual displacement applications, has been proposed for four field problems (thermo-magneto-electro-mechanical). The case of multilayered plates constituted by layers with mechanical, thermal, magnetic and electric properties has been considered in coupling. Finite element matrices have been derived in terms of a few "fundamental nuclei" by direct application of Carrera unified formulation in a new condensed form. A corresponding FEM code (called MUL2) has been build coherently with the presented formulation and applied to various multifield problems. Obtained results have shown the convenience of the proposed formulation as well as its capability to solve coupled problems by leading to quasi-three dimensional description of mechanical, thermal, magnetic and electrical variables in both static and dynamic cases. Future work could be directed to the extension to shell geometry.

Acknowledgement

This work has been carried out with the partial support of European Space Agency, ESTEC-Contract no. 21082/06/NL/PA.

References

[1] T. Ikeda, Fundamentals of Piezoelectricity, Oxford Science Publications, New York, 1996.
[2] E. Carrera, S. Brischetto, P. Nali, Variational statements and computational models for multifield problems and multilayered structures, Mechanics of Advanced Materials and Structures 15 (3) (2008) 182–198 (special issue).
[3] E. Carrera, Historical review of zig-zag theories for multilayered plates and shells, Applied Mechanics Review 56 (2003) 287–308.
[4] E. Carrera, S. Brischetto, Piezoelectric shell theories with a priori continuous transverse electromechanical variables, Journal of Mechanics of Materials and Structures 2 (2) (2007) 377–399.
[5] E. Carrera, C. Fagiano, Mixed piezoelectric plate elements with continuous transverse electric displacements, Journal of Mechanics of Materials and Structures 2 (3) (2007) 421–438.
[6] E.C.G.M. Kulikov, Finite deformation higher-order shell models and rigid-body motions, International Journal of Solids and Structures 45 (2008) 3153–3172.
[7] G.A. Altay, M.C. Dokmeci, Fundamental variational equations of discontinuous thermopiezoelectric fields, International Journal of Engineering Science 34 (7) (1996) 769–782.
[8] E. Carrera, M. Boscolo, A. Robaldo, Hierarchic multilayered plate elements for coupled multifield problems of piezoelectric adaptive structures: formulation and numerical assessment, Archives of Computational Method in Engineering 14 (2007) 383–430.
[9] Y. Jiashi, Electric, Optic and Acoustic Interactions in Crystals, Wiley, New York, 1979, p. 74.
[10] E. Carrera, Theories and finite elements for multilayered plates and shells: a unified compact formulation with numerical assessment and benchmarking, Archives of Computational Method in Engineering 10 (3) (2003) 215–296.
[11] E. Carrera, P. Nali, Description of a symbolic code able to calculate the unified formulation fundamental nuclei for PVD and RMVT variational statements, DIASP Internal Report, Politecnico di Torino, 2007.
[12] E. Carrera, L. DeMasi, Classical and advanced multilayered plate elements based upon PVD and RMVT. Part 2. Numerical implementations, International Journal of Numerical Methods in Engineering 55 (2002) 253–291.
[13] E. Carrera, M. Boscolo, Classical and mixed finite elements for static and dynamics analysis of piezoelectric plates, International Journal of Numerical Methods in Engineering 70 (2007) 253–291.
[14] E. Carrera, S. Brischetto, Analysis of thickness locking in classical, refined and mixed multilayered plate theories, Composite Structures 82 (2008) 449–562.
[15] K. Bhaskar, T.K. Varadan, J.S.M. Ali, Thermoelastic solutions for orthotropic and anisotropic composite laminates, Composites 27B (1996) 415–420.
[16] E. Carrera, Temperature profile influence on layered plates response considering classical and advanced theories, AIAA Journal 40 (9) (2002) 1885–1896.
[17] V. Tungikar, K. Rao, Three dimensional exact solution of thermal stresses in rectangular composite laminate, Composite Structures 27 (1994) 419–430.
[18] A. Robaldo, E. Carrera, A. Benjeddou, Unified formulation for finite element thermoelastic analysis of multilayered anisotropic composite plates, Journal of Thermal Stresses 28 (10) (2005) 1031–1065.
[19] P. Heyliger, D. Saravanos, Exact free-vibration analysis of laminated plates with embedded piezoelectric layers, Journal of Acoustical Society of America 98 (3) (1995) 1547–1557.
[20] E. Pan, Exact solution for simply supported and multilayered magneto-electro-elastic plates, Journal of Applied Mechanics 68 (2001) 608–618.
[21] E. Carrera, M.D. Gifico, P. Nali, S. Brischetto, Refined multilayered plate elements for coupled magneto-electro-elastic analysis, Multidiscipline Modeling in Materials and Structures 5 (2009) 119–138.